Room-temperature type-II multiferroic phase induced by pressure in cupric oxide

Noriki Terada[1], Dmitry D. Khalyavin[2], Pascal Manuel[2], Fabio Orlandi[2], Christopher J. Ridley[2], Craig L. Bull[2,3], Ryota Ono[4], Igor Solovyev[5,6,7], Takashi Naka[1], Dharmalingam Prabhakaran[8], and Andrew T. Boothroyd[8]

[1]*National Institute for Materials Science, Sengen 1-2-1, Tsukuba, Ibaraki 305-0047, Japan*

[2]*ISIS Facility, STFC Rutherford Appleton Laboratory, Chilton, Didcot, Oxfordshire, OX11 0QX, United Kingdom*

[3]*EaStCHEM School of Chemistry, The University of Edinburgh, King's Buildings, David Brewster Road, Edinburgh EH9 3FJ, United Kingdom*

[4]*Italian Institute of Technology, Via Morego, 30 16163 Genoa, Italy*

[5]*National Institute for Materials Science, MANA, 1-1 Namiki, Tsukuba, Ibaraki 305-0044, Japan*

[6]*Institute of Metal Physics, S. Kovalevskaya str. 18, 620108 Ekaterinburg, Russia*

[7]*Department of Theoretical Physics and Applied Mathematics, Ural Federal University, Mira str. 19, 620002 Ekaterinburg, Russia and*

[8]*Department of Physics, University of Oxford, Clarendon Laboratory, Parks Road, Oxford OX1 3PU, United Kingdom*

(Dated: July 16, 2022)

Abstract

According to previous theoretical work, the binary oxide CuO can become a room temperature multiferroic via tuning of the superexchange interactions by application of pressure. Thus far, however, there has been no experimental evidence for the predicted room-temperature multiferroicity. Here, we show by neutron diffraction that the multiferroic phase in CuO reaches 295 K with the application of 18.5 GPa pressure. We also develop a spin Hamiltonian based on density functional theory and employing superexchange theory for the magnetic interactions, which can reproduce the experimental results. The present study provides a stimulus to develop room-temperature multiferroic materials by alternative methods based on existing low temperature compounds, such as epitaxial strain, for tunable multifunctional devices and memory applications.

Magnetoelectric (ME) multiferroic materials exhibit both magnetic and ferroelectric properties simultaneously and have garnered significant attention owing to their remarkable physics of cross-correlated phenomena[1–4]. In particular, they can be used in the development of multistate memory devices with ME reading/writing operations.[5] In type-I multiferroics, ferroelectric and magnetic orderings appear at different temperatures, whereas ME orderings occur simultaneously in type-II multiferroics in which the ferroelectric polarization is induced by the loss of inversion symmetry at the magnetic ordering. Therefore, a strong coupling is expected between the magnetic and ferroelectric orderings. However, with rare exceptions,[7–13] the critical temperatures (T_C) in type-II multiferroics are far below room temperature, typically below $\sim$ 100 K.

One of the most promising solutions for resolving this limitation in type-II multiferroics involves increasing the T_C by strengthening the magnetic exchange interactions. This can be achieved by tuning the crystal structure using methods such as the application of pressure,[14, 15] strain,[16] or chemical substitution.[17] For Cu–O–Cu superexchange bonds in parent compounds of high-T_C superconductors, an exchange interaction J is on the order of 100 meV for a bond angle of $\sim$180°.[18] As this J value is considerably larger than that of most ionic antiferromagnets with smaller bond angles, the Néel temperature could be potentially increased even above room temperature by appropriately tuning the Cu–O–Cu bond angle in cuprates.

CuO exhibits a relatively high Néel temperature (T_{N2} =230 K) owing to its low-dimensional crystal structure (monoclinic $C2/c$[19]) with a Cu–O–Cu bond angle of 146°. The cuprate exhibits multiferroic behavior, wherein the ferroelectric polarization is induced by incommensurate (ICM) helical spin ordering (Fig. 1(a)) below $T_{\mathrm{N2}} = 230$ K.[20] Furthermore, CuO is a unique example of a chemically stable, binary oxide multiferroic material that is in contrast to alternative high-T_C multiferroics with complex chemical representations such as $Ba_{0.8}Sr_{1.2}Co_2Fe_{12-x}Al_xO_{22}$[12, 13] and $YBaCu_{1-x}Fe_xO_5$.[17] In fact, the multiferroic phases in these compounds can only be realized with phase coexistence in a metastable state.[12, 13, 17]

Using density functional theory (DFT) calculations, Rocquefelte et al. have predicted that the multiferroic phase of CuO can reach room temperature at pressure $P = 8.8$ GPa[14] or 40 GPa[15, 21], depending on the assumptions. Kozlenko et al. also reported DFT results, but concluded that the room temperature multiferroicity could not be achieved in

CuO.[22] These theoretical studies have encouraged experimentalists to investigate the evolution of the multiferroic phase of CuO with pressure using X-ray diffraction[22] and dielectric permittivity.[21, 23] However, owing to the lack of direct experimental evidence on the magnetic order parameters at pressures that could potentially stabilize the multiferroic phase at room temperatures, the influence of high pressure on the multiferroic state of CuO is not yet understood. In the present study, we used single crystal neutron diffraction to investigate the magnetic structure of CuO under high pressure and found that the multiferroic phase can be stabilized at room temperature, 295 K, at a pressure of 18.5 GPa. In addition, we have successfully reproduced the observed behavior by theoretical calculations based on DFT and superexchange theory.

At ambient pressure, below T_{N2} =230 K, helical spin order with the ICM magnetic propagation vector $\boldsymbol{k}_{\mathrm{ICM}} = (0.506, 0, -0.483)$ appears in CuO (Fig. 1(a))[24–27] concomitant with and coupled to a ferroelectric polarization along the b-axis.[28] In addition, the ICM ordering in the AF2 phase becomes the commensurate (CM) collinear spin ordering ($\boldsymbol{k}_{\mathrm{ICM}} = (0.5, 0, -0.5)$) at T_{N1} =213 K (Fig. 1(b)), and the ferroelectricity is not detected below T_{N1}. The pressure and temperature dependence of the dielectric permittivity was initially investigated in the low-pressure region up to 2.5 GPa. (Fig. 1(c)) The present results are consistent with the previous reports for the ambient and low pressure region.[21, 29] As the pressure increases, T_{N1} is diminished at the rate $dT_{\mathrm{N1}}/dP = -2.5$ K GPa^{-1}, whereas T_{N2} is increased by $dT_{\mathrm{N2}}/dP \simeq 3.4 \pm 0.2$ K GPa^{-1}, corresponding to the expansion of the multiferroic AF2 phase.(Fig. 1(d)) Several studies have demonstrated the existence of an additional phase (AF3) in an extremely narrow temperature range in the vicinity of the Néel temperature ($T \sim 230$ K),[30–32], which is a nonpolar/nonferroelectric ICM phase.[33] As the dielectric permittivity reflects the fluctuation of the electric dipole moments around the ferroelectric phase transition, the observed dielectic anomaly is considered to correspond to the ferroelectric phase transition at T_{N2}. To extend the study to higher pressures, neutron diffraction measurements were performed on single crystals in a Paris–Edinburgh (PE) cell with toroidal-profiled sintered diamond anvils on the WISH beamline at the ISIS Neutron and Muon Source facility in the UK. The experimental details are described in the Supplemental Material.[34]

Some typical neutron intensity maps for the ambient pressure $P = 0.5$ GPa are presented in Figs. 2(a) and 2(b), wherein a prominent peak at the CM position, $(1/2, 0, -1/2)$, was

observed at $T = 205$ K below $T_{\rm N1}$, whereas the peak position was observed at the ICM position, $(0.509, 0, -0.480)$, at $T = 214$ K, which is between $T_{\rm N1}$ and $T_{\rm N2}$. The split intensity distribution in the peaks is caused by crystal twinning in the sample used for the first experiment below 8.0 GPa. As displayed in Fig. 2(g), the CM peak intensity disappeared above $T \simeq 210$ K. Moreover, the intensity at the ICM position only existed within the temperature range of 210 K $\leq T \leq$ 232 K, and these results were consistent with those of previous neutron diffraction experiments conducted at ambient pressure.[24–27] The CM magnetic reflection at $(0.5, 0, -0.5)$ was observed up to 8.0 GPa, and $T_{\rm N1}$ decreases monotonically with increasing pressure(Figs. 2(c) and 2(g)-(j)). For example, the $T_{\rm N1}$ (= 185 K) at $P = 8.0$ GPa is reduced by 25 K from the ambient temperature value of 213 K. Above 8 GPa, the $T_{\rm N1}$ drops below the lowest attainable temperature of the experimental setup.

For the ICM AF2 phase, the ordering temperature $T_{\rm N2}$ increases almost linearly with the pressure and reaches room temperature ($T_{\rm N2}$ =295 K) at 18.5 GPa. This follows from the temperature dependence of the integrated intensity of the magnetic peak. (Fig. 2(n)). Thus, this is the first direct experimental evidence that the polar AF2 phase is stabilized at room temperature at pressure above 18.5 GPa, which implies that CuO can be a room-temperature type-II multiferroic under high pressure. The temperature versus pressure phase diagram of CuO was determined by plotting the phase transition temperatures at each measured pressure, as shown in Fig. 1(d). The pressure coefficient of $T_{\rm N2}$ was estimated as $dT_{\rm N2}/dP \simeq 3.4 \pm 0.2$ K GPa^{-1} by fitting the pressure variation of $T_{\rm N2}$, which is consistent with an earlier reported theoretical value $dT_{\rm N2}/dP \simeq 3.5 \pm 0.3$ K GPa^{-1}.[15]

For each pressure, the ICM $\boldsymbol{k}$-vector in the AF2 phase slightly depends on temperature as generally seen in intermediate temperature phases of frustrated magnetic systems.[35, 36] On the other hand, the $\boldsymbol{k}$-vector components substantially varied with the increasing pressure. For instance, the $\boldsymbol{k}$-vector is (0.509,0,-0.480) at ambient pressure, whereas it became $\boldsymbol{k} = (0.495, 0, -0.486)$ at 18.5 GPa. (see Fig. S1 in Supplemental Material[34]). The observed variation in the ICM $\boldsymbol{k}$-vector components is related to the pressure dependence of the magnetic exchange interactions, as we explain below.

Let us discuss what causes the large pressure dependence of the phase transition temperatures observed in the present neutron diffraction experiments, by means of DFT, which is

used for the construction of a realistic spin model

$$\mathcal{H}_{\mathrm{S}} = -\sum_{i>j} J_{ij} \boldsymbol{S}_i \cdot \boldsymbol{S}_j, \tag{1}$$

with $\boldsymbol{S}_i$ denoting spin 1/2 at the Cu site i. Subsequently, an effective Hubbard-type model was constructed for the magnetic Cu $3d$ states, and all model parameters were rigorously derived using DFT.[37, 38] All possible J_{ij} values were then evaluated in the framework of superexchange (SE) theory, to leading order in $\hat{t}_{ij}/U$ ($\hat{t}_{ij}$ and U are the effective intersite hopping and on-site Coulomb repulsion, respectively), which is the key theory for magnetic Mott insulators, such as CuO.[39] The basic difference from previous studies[14, 15, 22, 40] is that no assumptions were made regarding the form of J_{ij}, and all interactions were treated equally, with their strength determined by $\hat{t}_{ij}$ in the bonds. Furthermore, additional simplifications were eliminated while estimating T_{N2}, and a nonempirical random phase approximation (RPA) technique was used for the given set of parameters J_{ij} for each P.[44] To illustrate the robustness of the proposed model, two different implementations, Quantum ESPRESSO (QE) method with ultrasoft pseudopotentials [41], and the linear muffin-tin orbital (LMTO) method [42] were employed. The present theoretical approach has been successfully applied to other multiferroic systems.[43–47] More details of the calculation procedure are described in Supplemental Material.[34]

As illustrated in Figs. 3(a)-(e), we considered all the possible exchange interactions (with notation following Ref.[48]) for the bond distances up to 6.5 Å. Some of the interactions, J_{bc}, J_{abc}, and J_{2c}, were not considered in Ref. [15]. (see Table S1 in Supplemental Material[34]) Moreover, the exchange interactions with the same distances but different exchange paths in the ab-plane are not necessarily equivalent. Particularly, we take into account that $J_{ab} \neq J'_{ab}$ and $J_{2ab} \neq J'_{2ab}$. (Figs. 3(c)-(d)) As shown in Fig. 3(f), the AF interaction J'_{ac} along the $[10\bar{1}]$-direction is clearly the strongest. Then, J_{ac} operating in the "perpendicular" [101]-bond is substantially weaker than J'_{ac}, while J_{ab}, J_{2a}, J_b and J_{2ab} are negligibly small. Furthermore, we identify other sizable interactions J'_{ab}, J_{bc}, J_{abc}, J_{2c}, and J'_{2ab}, which contribute to the properties of CuO. The theoretical magnetic ground state could then be determined by minimizing the classical Heisenberg energy of Eq. (1) with respect to $\boldsymbol{k}$ and individual phases of spins in two Cu sublattices, which yields $\boldsymbol{k} = (0.516, 0, -0.493)$ (in QE). This is close to the experimental finding. A comparison of the present theoretical exchange parameters with previous inelastic neutron scattering results[48] confirmed that they are in good agreement

with each other, apart from the sign of J_{ac} (see Table S1 in Supplemental Material[34]). One of the other exchange parameters, J_{2c}, which was only introduced in the present study, could explain this experimental result. In the previous model, the FM J_{ac}, connecting the AFM chains running along the $[10\bar{1}]$-direction, is believed to be responsible for the FM coupling between the chains. (Fig. 3(a))[48] However, in the present work, J_{ac} is antiferromagnetic, and the FM coupling between the chains is stabilized by the AFM interaction J_{2c}, operating between the second neighbors in the ac-plane, which is substantially stronger than J_{ac}.

In order to further demonstrate the accuracy of our *ab initio* exchange parameters, we have calculated spin-wave dispersion relations with the exchange parameters obtained in the present work and those reported in the previous work.[21] As clearly seen in Fig. 2(a) in Supplemental Material[34], our *ab initio* exchange parameters reproduce the experimental spin-wave dispersion relation well, apart from the slightly overestimated interchain spectrum. On the other hand, the dispersion relation calculated with the exchange parameters given in Ref. [21] strongly overestimates the interchain spectrum. (Fig. 2(b) in Supplemental Material[34])

The strongest intra-chain interaction J'_{ac} was substantially changed by the application of pressure, from ~ -80 meV at ambient to ~ -128 meV at P =30 GPa (i.e., by a factor of 1.5; Fig. 4(a)). J'_{ac} was found to be almost linearly dependent on the angle Cu-O-Cu in the $[10\bar{1}]$-bond (inset of Figs. 4(a)), in contrast to the phenomenological rule (Ref. [49]) and one of the main assumptions made by Kozlenko et al.[22] The changes in the other parameters (Figs. 4(b)) appeared small on the scale of J'_{ac}. However, they were not negligible. For example, the ferromagnetic interaction J_{abc} increased by a factor of nearly four, the interactions J_{ac} and J_{bc} changed their signs, the AF interactions J_{2c} decreased by a factor of 2, and so on. Notably, by using the obtained parameters, the theoretical pressure dependence of $\boldsymbol{k}$ effectively reproduces the experimental trend, and at 20.5 GPa, $\boldsymbol{k} = (0.492, 0, -0.483)$ is obtained.

In the present theoretical analysis, with the parameters derived from the superexchange theory, the deviation of the spin-helix propagation vector was successfully reproduced at $\boldsymbol{k}$ =(1/2, 0, −1/2), which is in good agreement with the experimental results. Thus, although the anisotropic interactions may be responsible for the stability of the AF1 phase, the AF2 phase can be stabilized by isotropic exchange interactions alone, where the infinite degeneracy of the ground state proposed in Ref. [50] is lifted owing to the deviation from

$\boldsymbol{k}$ =(1/2, 0, −1/2). Moreover, $T_{\rm N2}$ increases linearly with pressure with the coefficient $dT_{\rm N2}/dP \sim 3.5$ K GPa^{-1} for both LMTO and QE calculations. This value is consistent with the experimental value of $dT_{\rm N2}/dP \simeq 3.4 \pm 0.2$ K GPa^{-1}, as well as $dT_{\rm N2}/dP \simeq 3.5 \pm 0.3$ K GPa^{-1} reported in Ref. [15]. Although the calculated value of $T_{\rm N2}$ at ambient pressure is somewhat larger than the experimental value, the present theoretical calculation successfully reproduced the tendency of pressure to stabilize the ICM AF2 phase. The 20 % difference in $T_{\rm N2}$ between the LMTO and QE results is caused by similar difference in the values of small exchange interaction operating between AF $[10\bar{1}]$ chains under high pressure, which are crucially important for establishing a non-zero $T_{\rm N2}$. [51]

Epitaxial strain modification of the lattice might be one of most promising alternative methods to realize room-temperature multiferroicity at ambient pressure in CuO. Our results show that the dominant exchange interaction in CuO, J'_{ac}, along the $[10\bar{1}]$ chain direction is significantly strengthened from -80 meV to -128 meV by tuning the Cu–O–Cu bond angle from 146° to 165°.(Fig. 4a) The Cu–Cu distance along the $[10\bar{1}]$ chain direction elongates by $\sim$ 3% and the b-axis diminishes by $\sim$ 10% with application of hydrostatic pressure of 18.5 GPa, which leads to the increase in the Cu–O–Cu bond angle. (see Table S2 in Supplemental Material[34]) However, Goswami et. al. recently reported a lower $T_{\rm N2}$ =175 K in the thin film on (001)MgO.[52] Nevertheless, there is a significant shift in $T_{\rm N2}$ from that of the bulk value at ambient pressure ($|\Delta T_{\rm N2}| = 55$ K); this shift is comparable to that at hydrostatic pressure $P = 18.5$ GPa in the bulk system of $|\Delta T_{\rm N2}| = 65$ K. Therefore, the quest to increase $T_{\rm N2}$ above room temperature via epitaxial thin film growth should focus on finding an appropriate substrate to enlarge the Cu–O–Cu bond angle. The application of chemical pressure (substitution) has also been attempted to stabilize the high-pressure phase at room temperature. However, these chemical substitutions reduce both $T_{\rm N1}$ and $T_{\rm N2}$ in CuO.[53–55]

Recently, J. S. Zhang et. al. have reported that T_C can be largely increased from 73.5 K to 162 K by application of pressure 4.5 GPa in the dielectric measurements on the type-II multiferroic $CuBr_2$.[56] Since $dT_C/dP \simeq 19.7$ K GPa^{-1} in $CuBr_2$, which is much larger than that in CuO (3.4 K GPa^{-1}), the multiferroic $CuBr_2$ is another candidate for room-temperature type-II multiferroicity induced by application of pressure. Theoretical investigations of other copper based compounds, CuX_2 and Cu_2OX_2 (X =halogen), have also predicted large pressure effects on the multiferroic phase stability.[57, 58]

In conclusion, magnetoelectric multiferroic research has been extensively carried out in the past 15 years from the perspectives of both basic physics and practical applications, wherein the latter is limited owing to the extremely low transition temperature of most type-II multiferroics. Here, it has been demonstrated by neutron diffraction that the multiferroic AF2 phase in CuO is stabilized at 295 K under high pressure (18.5 GPa). Moreover, we reconsidered the theoretical spin model of CuO using the DFT and nonempirical RPA techniques to appropriately model the impact of pressure on the transition temperature. The present theoretical calculations accurately reproduce the experimental results and improve the spin model by introducing the appropriate exchange interaction parameters. Ultimately, the multiferroic phase in CuO could be extended to room temperature under high pressure, and the pressure dependence could be successfully modeled. This study provides a path toward the development of multiferroic materials functioning under normal operating conditions for application in memory and other types of multifunctional devices.

ACKNOWLEDGMENTS

We would like to thank Takayuki Harada of National Institute for Materials Science for fruitful discussion, and Jérôme Debray and Claire V. Colin of the Institut Néel/CNRS for their technical support in cutting and polishing the crystals for the present neutron diffraction experiment. We acknowledge the STFC access to neutron beamtime. Raw data from the experiment can be obtained from https://doi.org/10.5286/ISIS.E.54807074. This work was supported by JSPS KAKENHI grants (No. 15H05433 and 17KK0099), JST-Mirai Program Grant Number JPMJMI18A3, Japan, the program AAAA-A18-118020190095-4 (Quantum), and the TUMOCS project, which has received funding from the European Union Horizon 2020 Research and Innovation Program under the Marie Sklodowska-Curie grant agreement (Grant No. 645660). We also would like to acknowledge the financial support from the Engineering and Physical Sciences Research Council, UK and Oxford-ShanghaiTech collaboration project.

[1] T. Kimura, T. Goto, H. Shintani, K. Ishizaka, T. Arima, Y. Tokura. *Nature* **426**, 55 (2003).

[2] S. W. Cheong, M. Mostovoy. *Nature Mater.* **6**, 13 (2007).

[3] Y. Tokura, S. Seki. *Adv. Mater.* **22**, 1554 (2010).

[4] Y. Tokura, S. Seki, N. Nagaosa. *Rep. Prog. Phys.* **77**, 076501 (2014).

[5] J. F. Scott. *Nat. Mater.* **6**, 256 (2007).

[6] D. I. Khomskii. *Physics* **2**, 20 (2009).

[7] Y. Kitagawa, Y. Hiraoka, T. Honda, T. Ishikura, H. Nakamura, T. Kimura *Nat. Mater.* **9**, 797 (2010).

[8] K. Okumura, T. Ishikura, M. Soda, T. Asaka, H. Nakamura, Y. Wakabayashi, and T. Kimura *Appl. Phys. Lett.* **98**, 212504 (2011).

[9] S. H. Chun, Y. S. Chai, B.-G. Jeon, H. J. Kim, Y. S. Oh, I. Kim, H. Kim, B. J. Jeon, S. Y. Haam, J.-Y. Park, S. H. Lee, J.-H. Chung, J.-H. Park, and K. H. Kim *Phys. Rev. Lett.* **108**, 177201 (2012).

[10] K. Okumura, K. Haruki, S. Hirose, T. Kimura. *Appl. Phys. Lett.* **103**, 032906 (2013).

[11] S. Hirose, K. Haruki, A. Ando, T. Kimura. *Appl. Phys. Lett.* **104**, 022907 (2014).

[12] T. Nakajima, Y. Tokunaga, M. Matsuda, S. Dissanayake, J. Fernandez-Baca, K. Kakurai, Y. Taguchi, Y. Tokura, T. H. Arima, *Phys. Rev. B* **94**, 195154 (2016).

[13] K. Kocsis, T. Nakajima, M. Matsuda, A. Kikkawa, Y. Kaneko, J. Takashima, K. Kakurai, T. Arima, F. Kagawa, Y. Tokunaga, Y. Tokura, and Y. Taguchi *Nat. Commun.* **10**, 1247 (2019).

[14] X. Rocquefelte, K. Schwarz, P. Blaha. *Sci. Rep.* **2**, 759 (2012).

[15] X. Rocquefelte, K. Schwarz, P. Blaha, S. Kumar, J. van den Brink. *Nat. Commun.* **4**, 3511 (2013).

[16] K. Shimamoto, S. Mukherjee, N. S. Bingham, A. K. Suszka, T. Lippert, C. Niedermayer, C. W. Schneider, *Phys. Rev. B* **95**, 184105 (2017).

[17] M. Morin, E. Canévet, A. Raynaud, M. Bartkowiak, D. Sheptyakov, V. Ban, M. Kenzelmann, E. Pomjakushina, K. Conder, and M. Medarde *Nat. Commun.* **7**, 13758 (2016).

[18] T. Shimizu, T. Matsumoto, T. Goto, K. Yoshimura, K. Kosuge. *J. Phys. Soc. Japan* **72**, 2165–2168 (2003).

[19] S. Åsbrink, L.-J. Norrby. *Acta Crystallogr. B* **26**, 8–15 (1970).

[20] T. Kimura, Y. Sekio, H. Nakamura, T. Siegrist, A. P. Ramirez. *Nature Mater.* **7**, 291 (2008).

[21] W. Lafargue-Dit-Hauret, D. Braithwaite, A. D. Huxley, T. Kimura, A. Saúl, X. Rocquefelte. *Phys. Rev. B* **103**, 214432 (2021).

[22] D. P. Kozlenko, K. Druzbicki, S. E. Kichanov, E. V. Lukin, H.-P. Liermann, K. V. Glazyrin,

B. N. Savenko. *Phys. Rev. B* **95**, 054115 (2017).

[23] R. Jana, P. Saha, V. Pareek, A. Basu, S. Kapri, S. Bhattacharyya, G. D. Mukherjee. *Sci. Rep.* **10**, 1038 (2016).

[24] B. X. Yang, T. R. Thurston, J. M. Tranquada, G. Shirane. *Phys. Rev. B* **39**, 4343 (1989).

[25] J. B. Forsyth, P. J. Brown, B. M. Wanklyn. Magnetism in cupric oxide. *J. Phys. C* **21**, 2917 (1989).

[26] P. J. Brown, T. Chattopadhyay, J. B. Forsyth, V. Nunez, Tasset. *J. Phys. Condens. Matter* **3**, 4281 (1991).

[27] M. Ain, A. Menelle, B. M. Wanklyn, E. F. Bertaut. *J. Phys. Condens. Matter* **4**, 5327 (1992).

[28] P. Babkevich, A. Poole, R. D. Johnston, B. Roessli, D. Prabhakaran and A. T. Boothroyd. Phys. Rev. B **85**, 134428 (2012).

[29] T. Chatterji, P. J. Brown, J. B. Forsyth. *J. Phys. Condens. Matter* **17**, S3057 (2005).

[30] R. Villarreal, G. Quirion, M. L. Plumer, M. Poirier, T. Usui, T. Kimura, *Phys. Rev. Lett.* **109**, 167206 (2012).

[31] A. Rebello, Z. C. M. Winter, S. Viall, J. J. Neumeier. *Phys. Rev. B* **88**, 094420 (2013).

[32] A. Wang, N. Qureshi, S. Yasin, A. Mukhin, E. Ressouche, S. Zherlitsyn, Y. Skourski, J. Geshev, V. Ivanov, M. Gospodinov, V. Skumryev *Nat. Commun.* **7**, 10295 (2016).

[33] N. Qureshi, E. Ressouche, A. Mukhin, M. Gospodinov, V. Skumryev. *Sci. Adv.* **6**, eaay7661 (2020).

[34] See Supplemental Material for the experimental details, theoretical calculation procedure, supplementary figure and tables.

[35] S. Mitsuda, N. Kasahara, T. Uno, and M. Mase1 J. Phys. Soc. Jpn. **67**, 4026 (1998).

[36] L. C. Chapon, G. R. Blake, M. J. Gutmann, S. Park, N. Hur, P. G. Radaelli, and S-W. Cheong Phys. Rev. Lett. **93**,177402 (2004).

[37] I. V. Solovyev, *J. Phys.: Condens. Matter* **20**, 293201 (2008).

[38] M. Imada and T. Miyake, J. Phys. Soc. Jpn. **79**, 112001 (2010).

[39] P. W. Anderson. *Phys. Rev.* **115**, 2 (1959).

[40] X. Rocquefelte, M. H. Whangbo, A. Villesuzanne, S. Jobic, F. Tran, K. Schwarz, P. Blaha *J. Phys. Condens. Matter* **21**, 045502 (2010).

[41] P. Giannozzi, S. Baroni, N. Bonini, M. Calandra, R. Car, C. Cavazzoni, D. Ceresoli, G. L. Chiarotti, M. Cococcioni *J. Phys.: Condens. Matter* **21**, 395502 (2009).

[42] O. K. Andersen. *Phys. Rev. B* **12**, 3060 (1975).

[43] I. V. Solovyev, Phys. Rev. B **87**, 144403 (2013).

[44] Solovyev, I. V., & Streltsov, S. V. *Phys. Rev. Materials* **3**, 114402 (2019).

[45] O. Besbes, S. Nikolaev, N. Meskini, and I. Solovyev, Phys. Rev. B **99**, 104432 (2019).

[46] Ono, R., Nikolaev, S., & Solovyev, I. *Phys. Rev. B* **102**, 064422 (2020).

[47] I. V. Solovyev, R. Ono, and S. Nikolaev, Phys. Rev. Lett. **127**, 187601 (2021).

[48] H. Jacobsen, S. M. Gaw, A. J. Princep, E. Hamilton, S. Tóth, R. A. Ewings, M. Enderle, E. M. Hétroy Wheeler, D. Prabhakaran, A. T. Boothroyd *Phys. Rev. B* **97**, 144401 (2018).

[49] T. Shimizu, T. Matsumoto, A. Goto, T. V. Chandrasekhar Rao, K. Yoshimura, K. Kosuge *Phys. Rev. B* **68**, 224433 (2003).

[50] G. Giovannetti, S. Kumar, A. Stroppa, J. vandenBrink, S. Picozzi, J. Lorenzana, *Phys. Rev. Lett.* **106**, 026401 (2011).

[51] N. D. Mermin and H. Wagner, Phys. Rev. Lett. **17**, 1133 (1966); **17**, 1307(E) (1966).

[52] S. Goswami, K. Dey, S. Chakraborty, S. Giri, U. Chowdhury, and D. Bhattacharya *ACS Omega* **5**, 22883 (2020).

[53] M. Ohashi, A. Tashiro, G. Oomi, X. G. Zheng. *Phys. Rev. B* **73**, 134421 (2006).

[54] J. Hellsvik, M. Balestieri, T. Usui, A. Stroppa, A. Bergman, L. Bergqvist, D. Prabhakaran, O. Eriksson, S. Picozzi, T. Kimura, and J. Lorenzana *Phys. Rev. B* **90**, 014437 (2014).

[55] N. V. P. Chaudhary, J. Krishna Murthy, A. Venimadhav. *Solid State Communications* **247**, 36 (2016).

[56] J. S. Zhang, Yiqi Xie, X. Q. Liu, A. Razpopov, V. Borisov, C. Wang, J. P. Sun, Y. Cui, J. C. Wang, X. Ren, Hongshan Deng, Xia Yin, Yang Ding, Yuan Li, J. G. Cheng, Ji Feng, R. Valentí, B. Normand, and Weiqiang Yu, Phys. Rev. Res. **2**, 013144 (2020).

[57] X. Rocquefelte, private communications.

[58] W. Lafargue-Dit-Hauret, Doctor Thesis (2018), University of Rennes 1, Modélisation des propriétés magnétiques et multiferroïques d'oxydes de cuivre

FIGURES

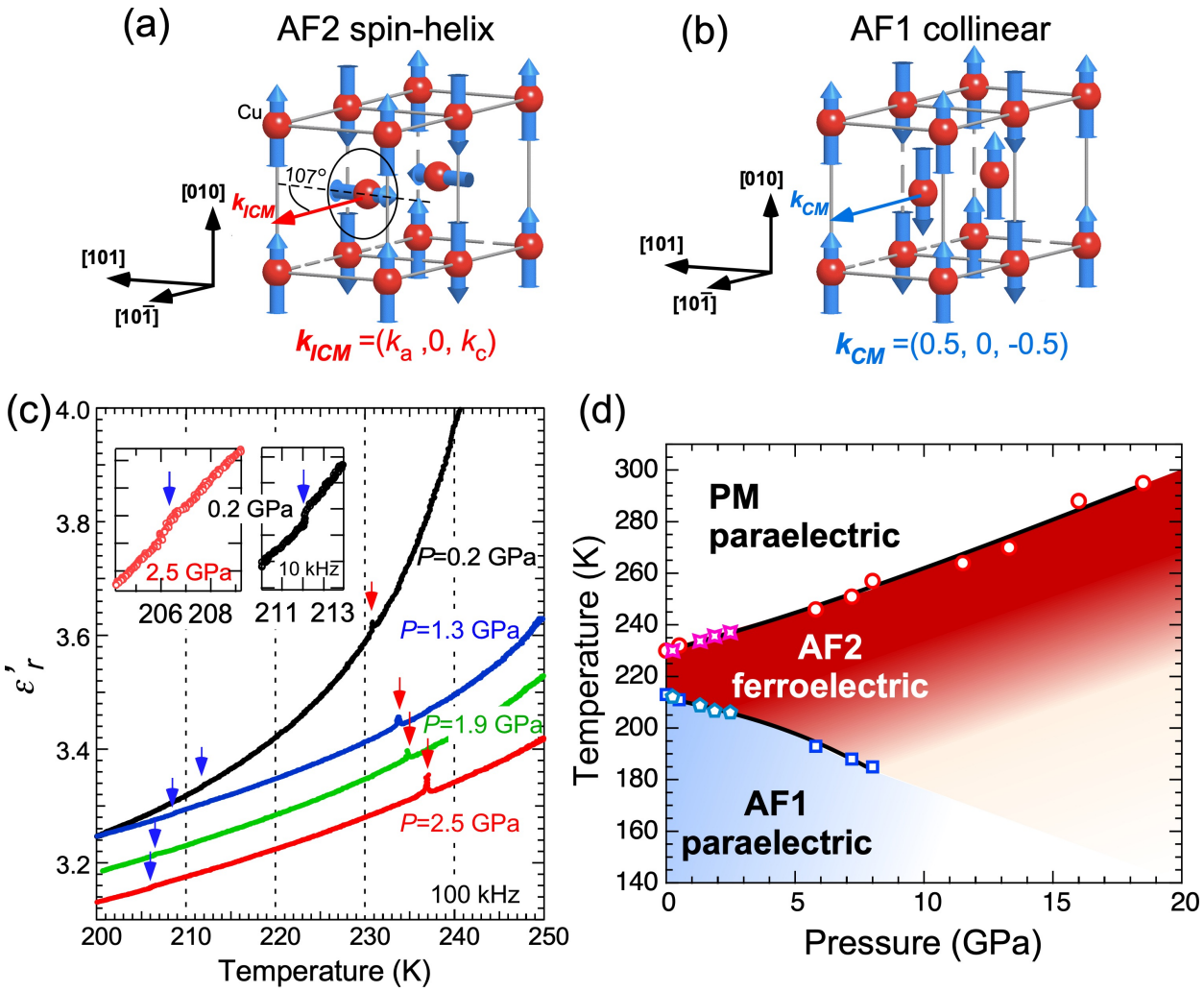

FIG. 1. Schematics of (a)spin-helix structure with incommensurate $\boldsymbol{k}_{\mathrm{ICM}} = (k_a, 0, k_c)$ in the AF2 phase (the angle between $\boldsymbol{k}_{\mathrm{ICM}}$ and the spiral plane is $\sim 107°$), and (b)collinear structure with commensurate $\boldsymbol{k} = (0.5, 0, -0.5)$ in the AF1 phase. (c) Pressure dependence of the real part of the relative dielectric permittivity of CuO. Inset shows an expansion around lower phase transition temperature T_{N1} at 0.2 GPa and 2.5 GPa. (d) Temperature versus pressure phase diagram of multiferroic CuO. Square (circle) and pentagon (star) symbols denote phase transition temperature points of $T_{\mathrm{N1}}(T_{\mathrm{N2}})$ determined by neutron diffraction and dielectric permittivity experiments, respectively.

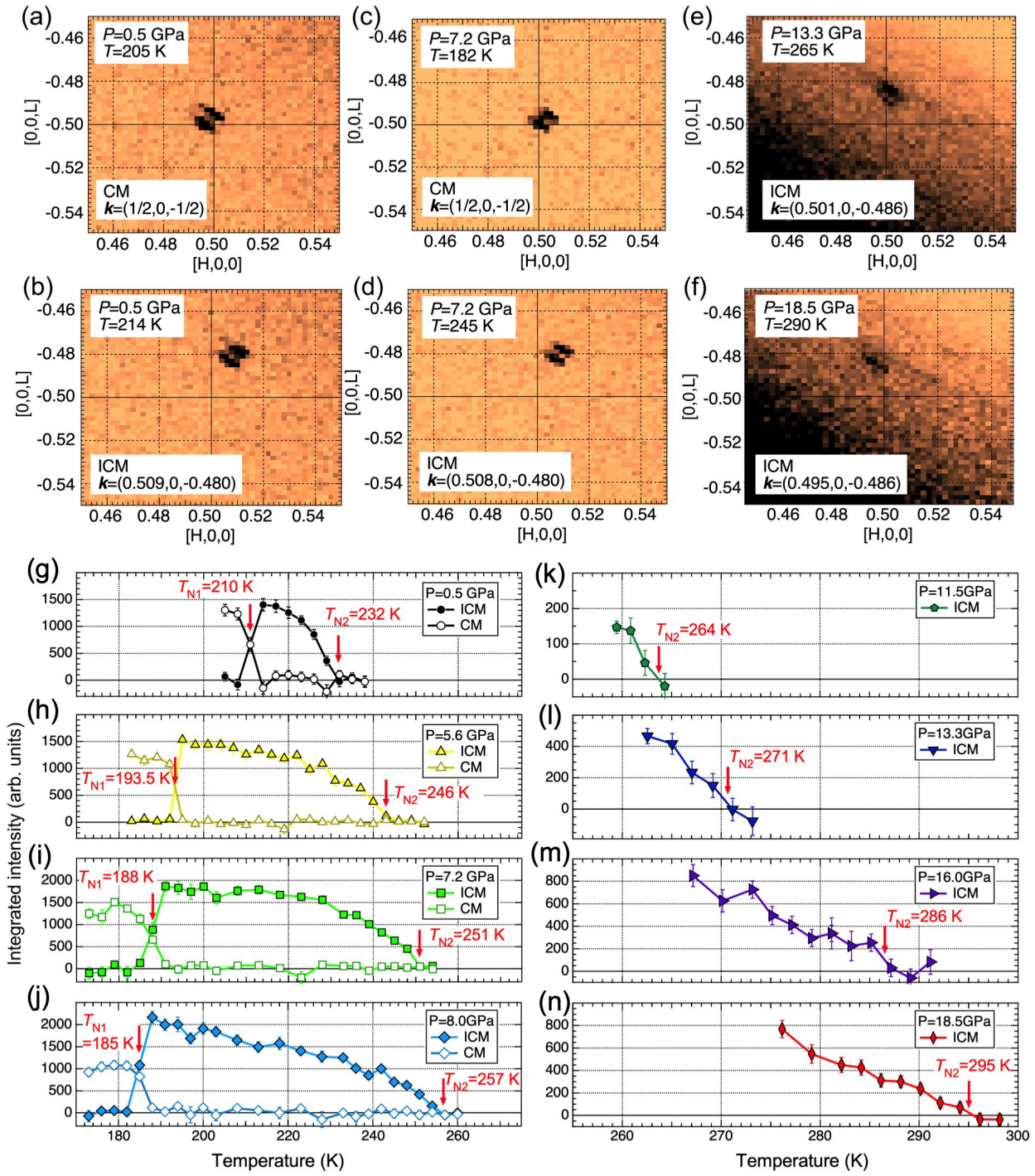

FIG. 2. (a-f) Neutron diffraction intensity maps near reciprocal lattice position, $\boldsymbol{Q} = (0.5, 0, -0.5)$ in the $(H, 0, L)$ plane, measured at typical pressures and temperatures. (g-n) Plots depict integrated intensities of magnetic Bragg reflections associated with commensurate $\boldsymbol{k} = (0.5, 0, -0.5)$ (open symbol) and incommensurate $\boldsymbol{k} = (k_a, 0, k_c)$ magnetic phases for typical pressures and temperatures.

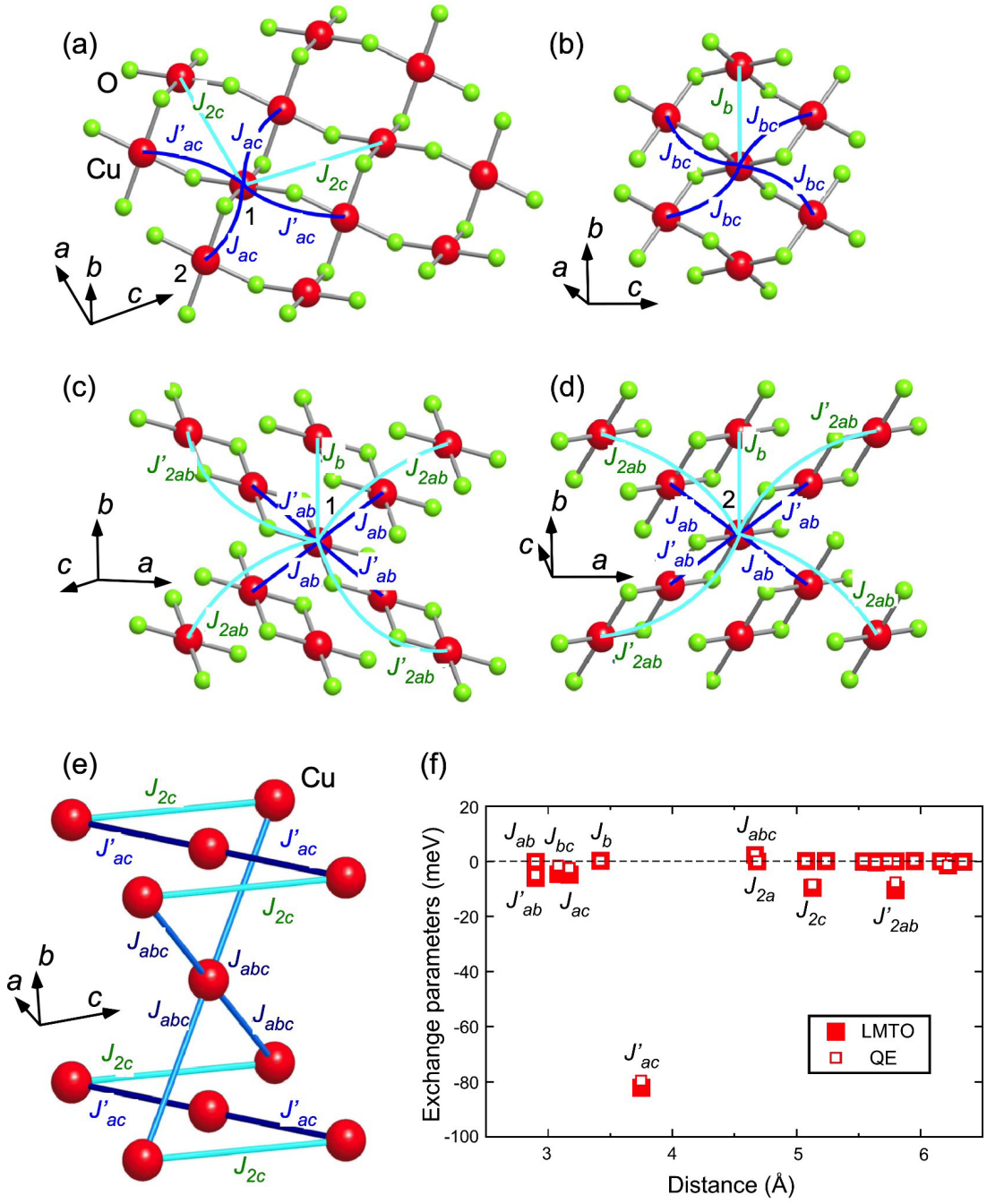

FIG. 3. Superexchange interaction paths (a) in the ac plane, (b) the bc plane, and (c,d) in the ab plane around Cu sites 1 and 2. (e) Long-range interactions J_{abc} between the ac planes. (f)Distance dependence of isotropic superexchange interactions, as obtained in the QE and LMTO methods at ambient pressure.

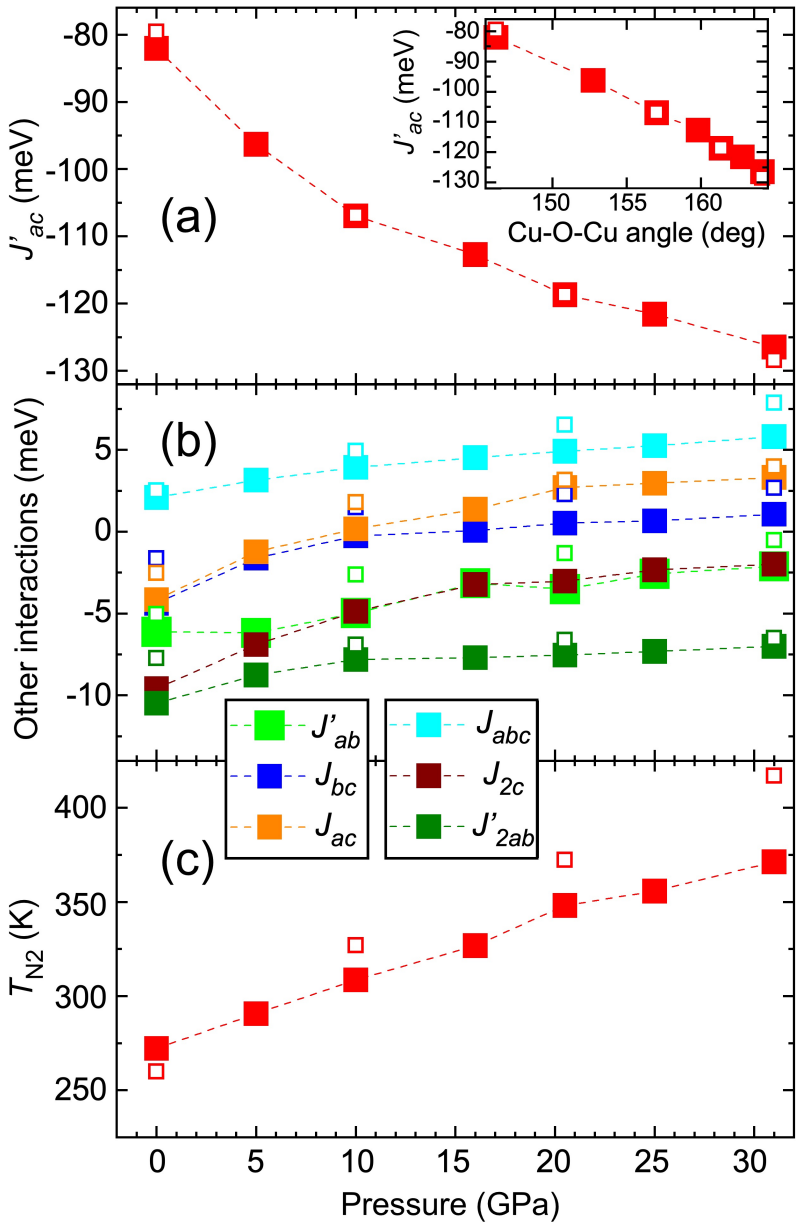

FIG. 4. Pressure dependence of (a) J'_{ac}, (b) J'_{ab}, J_{bc}, J_{ac}, J_{abc}, J_{2c}, and J'_{2ab}, and (c) $T_{\rm N2}$. Closed and open symbols show the results of the LMTO and QE calculations, respectively. The notations for the parameters are shown in Fig. 3. The inset in (a) shows the dependence of J'_{ac} on the angle Cu-O-Cu.